PERGAMON

Available online at www.sciencedirect.com

SCIENCE DIRECT®

Polyhedron 22 (2003) 2487–2497

POLYHEDRON

www.elsevier.com/locate/poly

Molecular magnets based on $M(hfac)_2$ and spin-labeled nitrile

O.V. Koreneva [a], G.V. Romanenko [b], Yu. G. Shvedenkov [a], V.N. Ikorskii [b], V.I. Ovcharenko [b,*]

[a] *Novosibirsk State University, Pirogova Street 2, 630090 Novosibirsk, Russia*
[b] *International Tomography Center, Russian Academy of Sciences, Institutskaya Street 3A, 630090 Novosibirsk, Russia*

Received 19 November 2002; accepted 17 January 2003

Abstract

Syntheses, structure, and magnetic properties of $[Cu(hfac)_2]_2L$, $Cu(hfac)_2L$, and $[M(hfac)_2]_3L_2$, where M = Mn, Co, are described. Special attention is paid to the unusual structure of the two polymorphs of $Cu(hfac)_2L$ and to the magnetic properties of $[M(hfac)_2]_3L_2 \cdot 0.5C_7H_{16}$, for which a magnetic phase transition to the ferromagnetic state has been found.

Keywords: Molecular magnets; Copper(II); Manganese(II); Cobalt(II); Nitroxide; Magnetic exchange coupling

1. Introduction

Previously, we described a modified synthesis and the structure of spin-labeled nitrile NIT-CN [1]. The structure of the NIT-CN molecule possessing reasonably high symmetry (2*mm*) seemed to be favorable for the formation of highly dimensional structures in reactions with hexafluoroacetylacetonates ($M(hfac)_2$). However, we failed to isolate any of the complexes $M(hfac)_2$ (M = Cu, Ni and Co) with NIT-CN. The nitrile group in the 2 position of the heterocycle probably decreases the donor ability of the oxygen atoms of the nitronylnitroxide fragment, which is weak in itself. Moreover, structure simulation showed that simultaneous coordination of nitronylnitroxide oxygens and the nitrile nitrogen by two hexafluoroacetylacetonate matrices is sterically hindered. This prompted us to study the possibility of synthesizing highly dimensional heterospin complexes using 2-(4′-cyanophenyl)-4,4,5,5-tetramethyl-2-imidazoline-3-oxide-l-oxyl (L), where the lengthening of the side chain removes steric limitations on the construction of *n*-dimensional heterospin systems with connectivity 3. For L, connectivity 3 is realized in the case of coordination of the O atoms of the two N–O groups and the nitrile N atom (Scheme 1). Scheme 1 shows a number of variants of complementing chain (a) by metal-containing matrices (in Scheme 1, the $M(hfac)_2$ matrices are denoted by circles, and the ⊢ fragment is the model of tridentate nitronylnitroxide). Chain (a) may be simply complemented by metal-containing matrices (case b), leading to compounds with the following stoichiometry: $M(hfac)_2/L = 2/1$. Among highly dimensional structures, the structures corresponding to heterospin complexes with stoichiometry 3/2 are ladder (c) or layered polymer (d). While investigating mixed-ligand complexes of $M(hfac)_2$ with L, we found that $Cu(hfac)_2$ forms only polymer chains (of a or b type), whereas $M(hfac)_2$, where M = Mn, Co, form layered polymer (d) magnets. This work investigates syntheses, structure, and magnetic properties of these compounds.

* Corresponding author. Fax: +7-3832-33-1399.
E-mail address: ovchar@tomo.nsc.ru (V.I. Ovcharenko).

0277-5387/03/$ - see front matter
doi:10.1016/S0277-5387(03)00229-8

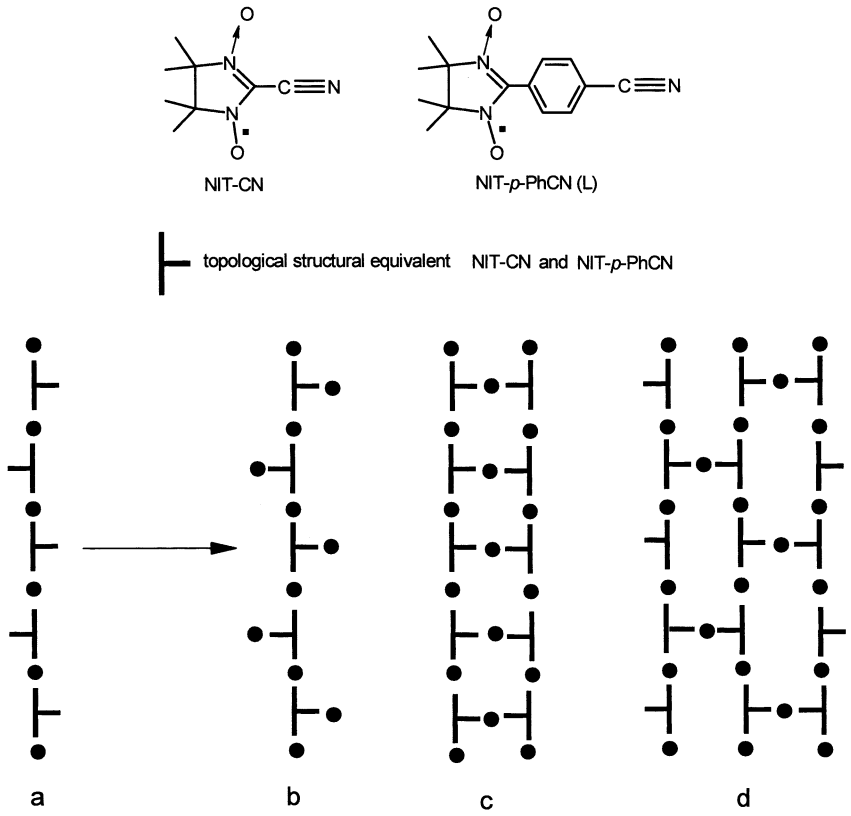

Scheme 1.

2. Experimental

2.1. Syntheses of nitroxides and complexes

2.1.1. 2-(4′-Cyanophenyl)-4,4,5,5-tetramethyl-2-imidazoline-3-oxide-l-oxyl (L)

2,3-bis-Hydroxylamino-2,3-dimethylbutane sulfate monohydrate (5 g) [2,3] was placed in a flask, and water (50 ml) and 4-cyanobenzaldehyde (2.5 g) were added. The reaction mixture was stirred for 2 h. This gave a transparent yellow solution, to which dry Na_2CO_3 ($\sim$2 g) was added in portions with vigorous stirring to pH $\sim$ 7. The white precipitate was filtered off, washed with water, and dried first in a flow of air and then in a vacuum desiccator for 5 h at 30 °C. To the resulting 1,3-dihydroxyimidazolidine (2.5 g) was added $CHCl_3$ (100 ml). The mixture was cooled to $\sim$5 °C, and a solution of $NaIO_4$ (2.84 g) in water (70 ml) was added with stirring. The organic layer colored deep violet blue. After 1.5 h, the organic layer was separated. The aqueous phase was treated with several 30–40 ml portions of $CHCl_3$ to practically complete decolorization. The chloroform extracts were consolidated, dried over $CaCl_2$, evaporated to a small amount, and purified by column chromatography on Al_2O_3 ($CHCl_3$ as eluent). The violet blue fraction was collected, evaporated to 15–20 ml, and diluted with an equal amount of hexane. After 15–20 min, the L precipitate was filtered off, washed with cold hexane, and dried in air. Yield: 5.25 g, 75%. Calc. for $C_{14}H_{16}N_3O_2$: C 65.1, H 6.2, N 16.3%; Found: C 65.3, H 6.4, N 16.3%.

2.1.2. Cu(hfac)$_2$L (α- and β-polymorphs)

A mixture of $Cu(hfac)_2$ (0.0478 g, 10^{-4} mol) and L (0.0259 g, 10^{-4} mol) was dissolved with stirring in hot (50 °C) heptane (40 ml). The reaction mixture was filtered and cooled to room temperature. After 2–3 h, dark violet blue needle crystals of β-$Cu(hfac)_2L$ precipitated, which were filtered off, washed with cold heptane, and dried in a flow of air. Yield: 0.035 g, 48%. Calc. for $CuC_{24}H_{18}N_3O_6F_{12}$: C 39.1, H 2.7, N 5.8%; Found: C 38.9, H 2.6, N 5.8%. After the filtrate was kept for 1 day, thin dark violet blue plates of α-$Cu(hfac)_2L$ crystals precipitated, which were mechanically separated from the minor impurity of needle crystals of β-$Cu(hfac)_2L$. Yield: 0.026 g, 35%. Calc. for $CuC_{24}H_{18}N_3O_6F_{12}$: C 39.1, H 2.7, N 5.8%; Found: C 38.9, H 2.9, N 5.4%.

2.1.3. [Cu(hfac)$_2$]$_2$L

Heptane (35 ml) was poured on a mixture of $Cu(hfac)_2$ (0.0955 g, 2×10^{-4} mol) and L (0.0259 g, 10^{-4} mol). The reaction mixture was stirred for 30 min at 50 °C till the starting reagents completely dissolved.

Table 1
Crystal data and experimental details

	Compound				
	$[Co(hfac)_2]_3L_2\cdot 0.5C_7H_{16}$	$[Mn(hfac)_2]_3L_2\cdot 0.5C_7H_{16}$	α-$Cu(hfac)_2L$	β-$Cu(hfac)_2L$	$[Cu(hfac)_2]_2L$
Space group	$P\bar{1}$	$P\bar{1}$	$P\bar{1}$	$P2_1/c$	$P\bar{1}$
Unit cell parameter					
a (Å)	12.593(3)	12.742(3)	11.431(2)	9.854(2)	13.043(3)
b (Å)	12.726(3)	12.832(3)	12.317(3)	34.522(7)	13.872(3)
c (Å)	15.016(3)	15.073(3)	12.682(3)	9.607(2)	15.061(3)
α (°)	112.81(3)	113.06(2)	91.05(3)		104.87(3)
β (°)	99.42(3)	99.61(1)	107.13(3)	113.07(3)	107.02(3)
γ (°)	101.29(3)	100.95(2)	116.26(3)		107.14(3)
V (Å^3)	2097.5(7)	2145.4(8)	1507.1(5)	3007(1)	2308.0(8)
Z, D_{calc} (g cm^{-3})	1, 1.618	1, 1.607	2, 1.622	4, 1.626	2, 1.746
μ (mm^{-1})	0.730	0.574	0.841	0.843	1.073
θ collection (°)	$1.79 < \theta < 25.00$	$1.78 < \theta < 25.01$	$1.8 < \theta < 25.00$	$2.25 < \theta < 25.00$	$1.53 < \theta < 25.05$
I_{hkl} coll/uniq	7455/7099	7564/7204	5036/4777	5635/5303	8290/7907
R_{int}	0.0673	0.0519	0.0418	0.0580	0.0687
I_{hkl}/N	7099/806	7204/834	4777/545	5303/479	7907/728
Goof (F^2)	0.972	1.118	1.005	0.952	0.982
R_1 ($I > 2\sigma(I)$)	0.0513	0.0925	0.0649	0.0767	0.0791
wR_2	0.1111	0.2520	0.1723	0.1597	0.1873
R_1 for all data	0.1516	0.1518	0.1327	0.2986	0.1884
wR_2	0.2321	0.2988	0.2119	0.2604	0.2448

Then it was filtered, cooled to room temperature, and kept for 15 h. The dark violet blue plate-like crystals were filtered off, washed with cold heptane, and dried in air. Yield: 0.079 g, 65%. Calc. for $Cu_2C_{34}H_{20}N_3O_{10}F_{24}$: C 33.5, H 2.0, N 3.5%; Found: C 33.0, H 2.2, N 3.6%.

2.1.4. $[Co(hfac)_2]_3L_2\cdot 0.5C_7H_{16}$

A mixture of $Co(hfac)_2\cdot 2H_2O$ (0.0763 g, 1.5×10^{-4} mol) and L (0.0259 g, 10^{-4} mol) was dissolved in boiling CH_2Cl_2 (15 ml). The solution was filtered and cooled to room temperature; then heptane (20 ml) was added. After 1 day, the brown–red crystals were filtered off, washed with cold heptane, and dried in air. Yield: 0.063 g, 62%. Calc. for $Co_3C_{58}H_{38}N_6O_{16}F_{36}$: C 36.0, H 2.0, N 4.3%; Found: C 36.3, H 2.0, N 4.9%.

2.1.5. $[Mn(hfac)_2]_3L_2\cdot 0.5C_7H_{16}$

The Mn(II) complex was synthesized by the procedure completely analogous to the procedure for the preparation of $[Co(hfac)_2]_3L_2\cdot 0.5C_7H_{16}$. $[Mn(hfac)_2]_3L_2\cdot 0.5C_7H_{16}$ is obtained as dark green crystals. Yield: 0.059 g, 56%. Calc. for $Mn_3C_{58}H_{38}N_6O_{16}F_{36}$: C 36.2, H 2.0, N 4.4%; Found: C 36.8, H 2.0, N 3.9%.

Perfectly faceted crystals of $Cu(hfac)_2L$ (α-, β-polymorphs) or $[Cu(hfac)_2]_2L$ suitable for X-ray analysis crystallize on cooling from heptane solutions containing $Cu(hfac)_2$ and L in a ratio of 1/1 or 2/1, respectively. Using other reagent ratios leads to precipitation of a mixture of crystals of these complexes. No other compounds of $Cu(hfac)_2$ with L have been recorded. On the contrary, the reaction of $M(hfac)_2$ (M = Mn, Co) with L with any reagent ratio in solution led only to solid complexes with stoichiometry $M(hfac)_2/L = 3/2$. The complexes are insoluble in hydrocarbons. Therefore single crystals of $[M(hfac)_2]_3L_2\cdot 0.5C_7H_{16}$ were grown from a CH_2Cl_2/heptane mixture.

Table 2
Selected bond lengths (Å) and angles (°) in α-$Cu(hfac)_2L$ and β-$Cu(hfac)_2L$

α-$Cu(hfac)_2L$		β-$Cu(hfac)_2L$	
Bond lengths			
Cu–O(1)	1.914(7)	Cu(1)–O(1)	1.933(5)
Cu–O(2)	1.919(7)	Cu(1)–O(2)	1.954(5)
Cu–O(4)	1.930(8)	Cu(2)–O(3)	1.923(5)
Cu–O(3)	1.932(7)	Cu(2)–O(4)	1.927(5)
Cu–O(5)	2.488(10)	Cu(1)–O(01)	2.414(5)
Cu–O(6′)	2.697(9)	Cu(2)–O(02)	2.638(5)
O(5)–N(1)	1.26(1)	O(01)–N(1)	1.294(6)
N(2)–O(6)	1.29(1)	N(2)–O(02)	1.265(7)
N(1)–C(17)	1.36(1)	N(1)–C(03)	1.333(8)
N(2)–C(17)	1.33(1)	N(2)–C(03)	1.351(8)
C(21)–C(24)	1.45(2)	C(07)–C(010)	1.45(1)
C(24)–N(3)	1.13(1)	C(010)–N(3)	1.13(1)
Bond angels			
O(1)–Cu–O(2)	93.2(3)	O(1)–Cu(1)–O(2)	92.4(2)
O(4)–Cu–O(3)	92.2(3)	O(3)–Cu(2)–O(4)	92.9(2)
O(5)–Cu–O(6)	148.4(3)		
N(1)–O(5)–Cu	150.6(7)	N(1)–O(01)–Cu(1)	125.5(4)
N(2)–O(6)–Cu′	149.4(7)	N(2)–O(02)–Cu(2)	150.8(4)

Table 3
Selected bond lengths (Å) and angles (°) in $[Cu(hfac)_2]_2L$

$[Cu(hfac)_2]_2L$					
Bond lengths					
Cu(1)–O(1)	1.952(7)	Cu(2)–O(5)	1.916(6)	Cu(3)–O(8)	1.931(6)
Cu(1)–O(2)	1.912(6)	Cu(2)–O(6)	1.941(7)	Cu(3)–O(7)	1.935(6)
Cu(1)–O(3)	1.935(7)	Cu(2)–O(9)	2.530(7)	Cu(3)–O(10)	2.637(7)
Cu(1)–O(4)	1.945(7)				
Cu(1)–N(1)	2.233(9)				
Bond angles					
O(3)–Cu(1)–O(4)	92.4(3)	O(5)–Cu(2)–O(6)	93.1(3)	O(8)–Cu(3)–O(7)	92.5(3)
O(2)–Cu(1)–O(1)	92.1(3)	N(2)–O(9)–Cu(2)	152.7(6)	N(3)–O(10)–Cu–(3)	138.6(6)
O(3)–Cu(1)–N(1)	87.9(3)				
C(21)–N(1)–Cu(1)	163.6(9)				

Table 4
Selected bond lengths (Å) and angles (°) in $[Mn(hfac)_2]_3L_2\cdot 0.5C_7H_{16}$

$[Co(hfac)_2]_3L_2\cdot 0.5C_7H_{16}$		$[Mn(hfac)_2]_3L_2\cdot 0.5C_7H_{16}$	
Bond lengths			
Co(1)–O(1)	2.043(6)	Mn(1)–O(1)	2.130(5)
Co(1)–O(2)	2.027(5)	Mn(1)–O(2)	2.122(5)
Co(1)–O(7)	2.150(6)	Mn(1)–O(7)	2.180(5)
Co(2)–O(3)	2.054(5)	Mn(2)–O(4)	2.110(5)
Co(2)–O(4)	2.020(6)	Mn(2)–O(3)	2.141(5)
Co(2)–O(8)	2.170(5)	Mn(1)–O(8)	2.187(5)
Co(3)–O(5)	2.043(6)	Mn(2)–O(5)	2.136(6)
Co(3)–O(6)	2.065(6)	Mn(3)–O(6)	2.135(6)
Co(3)–N(3)	2.130(7)	Mn(3)–N(3)	2.246(8)
O(7)–N(1)	1.275(7)	O(7)–N(1)	1.300(7)
N(2)–O(8)	1.277(7)	N(2)–O(8)	1.288(7)
N(1)–C(22)	1.347(9)	N(1)–C(22)	1.324(9)
N(2)–C(22)	1.374(9)	N(2)–C(22)	1.363(8)
C(29)–N(3)	1.117(9)	C(29)–N(3)	1.137(11)
C(26)–C(29)	1.463(12)	C(26)–C(29)	1.421(12)
Bond angles			
O(2)–Co(1)–O(1)	87.4(2)	O(2)–Mn(1)–O(1)	82.7(2)
N(1)–O(7)–Co(1)	129.3(5)	N(1)–O(7)–Mn(1)	130.2(4)
O(4)–Co(2)–O(3)	87.6(2)	O(4)–Mn(2)–O(3)	82.8(2)
N(2)–O(8)–Co(2)	127.6(5)	N(2)–O(8)–Mn(2)	128.5(4)
O(5)–Co(3)–O(6)	88.4(2)	O(5)–Mn(3)–O(6)	84.3(2)
C(29)–N(3)–Co(3)	173.6(9)	C(29)–N(3)–Mn(3)	172.9(9)

2.2. X-ray crystallography

For all single crystals, the data were collected on a Bruker AXS P4 automatic diffractometer at room temperature using the standard procedure (Mo radiation, $\theta/2\theta$ scan mode, $V_{min} = 3^\circ$ min^{-1}, $2.34 < \theta < 25.02^\circ$). The structures were solved by direct methods. The full-matrix least-squares refinement was carried out anisotropically for nonhydrogen atoms and isotropically for hydrogen atoms. Some atoms were localized theoretically. All structure solution and refinement calculations were fulfilled with SHELX-97. The main crystal data for the compounds and details of experiment are listed in Table 1; selected bond lengths and angles are given in Tables 2–4.

2.3. Magnetic measurements

Magnetic measurements were fulfilled on a SQUID (Quantum Design) magnetometer in the temperature range 2–300 K in an external magnetic field of up to 30 kOe. Molar magnetic susceptibility (χ) was calculated by applying corrections for atomic diamagnetism using Pascal's scheme. In the paramagnetic region, the effective magnetic moment was evaluated by the formula $\mu_{eff} = [(3k/N_A\beta^2)\chi T]^{1/2} \approx (8\chi T)^{1/2}$, where k is Boltzmann's constant, N_A is the Avogadro number, and β is the Bohr magneton. The magnetic phase transition temperature was determined as an extremum of magnetic susceptibility with respect to temperature $\partial\chi/\partial T$.

3. Results and discussion

3.1. Structure of compounds

The crystals of all Cu(II) complexes are formed by polymer chains (Figs. 1 and 2), in which the $\{Cu(hfac)_2\}$ fragments are linked via the NO oxygen atoms of L. In solid β-$Cu(hfac)_2L$ and $[Cu(hfac)_2]_2L$ the environment of Cu atoms in CuO_6 coordination polyhedra is centrosymmetric (square bipyramid), whereas in α-$Cu(hfac)_2L$ it is acentric (Tables 2 and 3). The hfac O atoms lie in the equatorial plane, the Cu–O distances being up to 1.912–1.954 Å. The axial Cu–O distances are long enough: 2.414–2.697 Å. The chain of β-$Cu(hfac)_2L$ consists of alternating centrosymmetric bipyramids with the axial distances of 2.414 and 2.638 Å. On the contrary, in the chain of the α-modification, the axial Cu–O bond lengths in the coordination units differ (2.488 and 2.697 Å). As in the chains of the β-modification, in the chains of $[Cu(hfac)_2]_2L$ and in

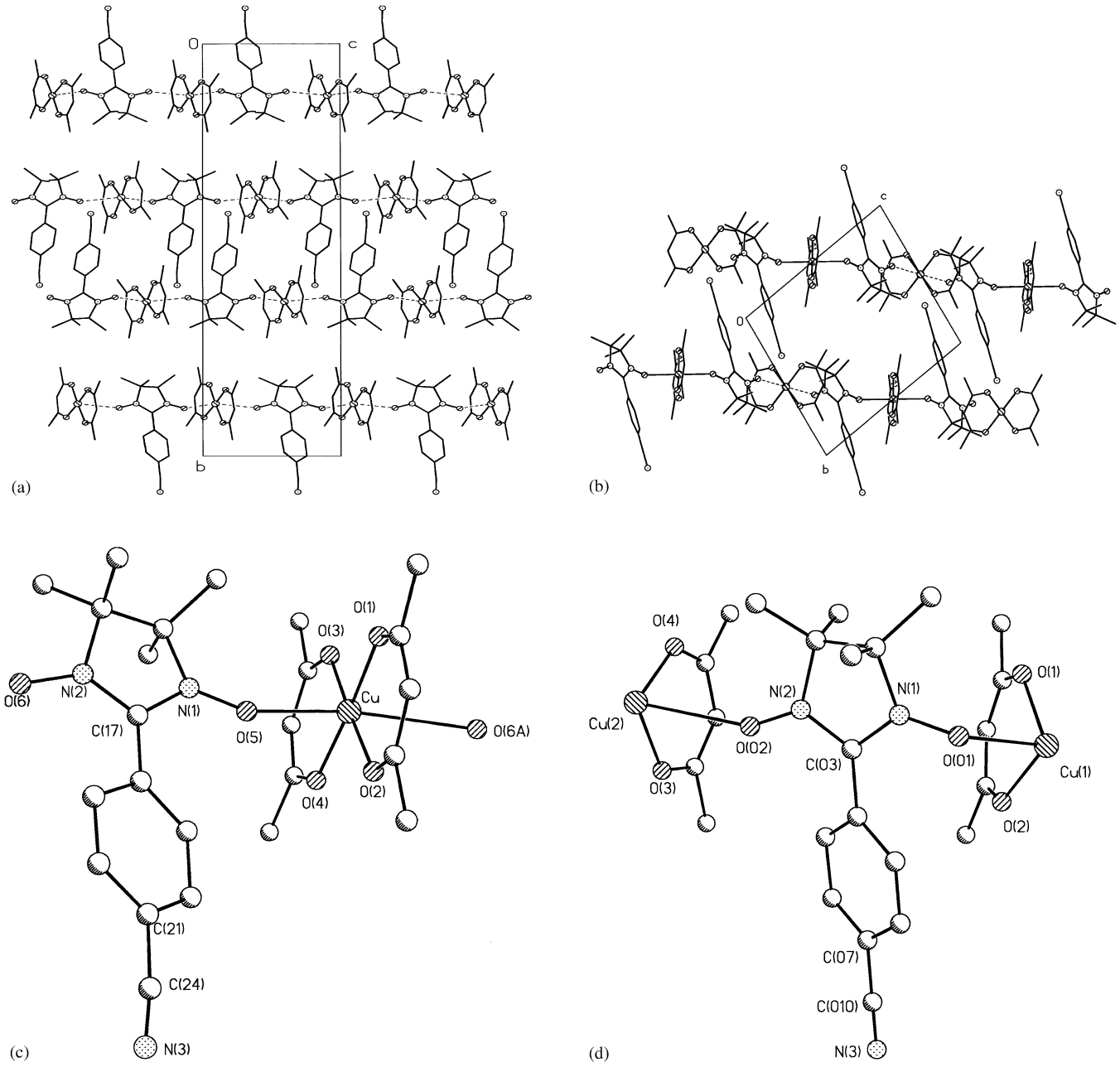

Fig. 1. Chain packing and atom numbering scheme in the crystal structure of the α-$Cu(hfac)_2L$ (a, c) and β-$Cu(hfac)_2L$ (b, d) polymorphs.

symmetric CuO_6 units, the axial bond lengths alternate (2.530 and 2.637 Å). The environment of the 'terminal' Cu atom in $[Cu(hfac)_2]_2L$ is a square pyramid with an apical N atom (Fig. 2). The Cu–N distance is 2.233 Å. As a result, in $[Cu(hfac)_2]_2L$, the paramagnetic ligand is bridging tridentate. Note that in β-$Cu(hfac)_2L$ and $[Cu(hfac)_2]_2L$ one can simultaneously observe the centrosymmetric character of CuO_6 polyhedra and the alternating arrangement of {–*p*-PhCN} fragments relative to the chain axis (Fig. 1(b) and Fig. 2), whereas in α-$Cu(hfac)_2L$, the {–*p*-PhCN} fragments lie on one side of the chain (Fig. 1(a)). In the structure of α-$Cu(hfac)_2L$, the neighboring chains are antiparallel, forming ribbons (Fig. 1(a)). Inside the ribbons, the shortest contacts are F···F 2.83–2.86 Å (the shortest distances between the F atoms of the neighboring ribbons are at least 3.1 Å).

In the isostructural compounds $[M(hfac)_2]_3L_2 \cdot 0.5C_7H_{16}$ (M = Co, Mn), the coordination polyhedra of the three crystallographically independent metal atoms are centrosymmetric octahedra (Fig. 3). The equatorial plane here is formed by the O atoms of two hfac, and the axial positions are occupied by the NO oxygen atoms or N_{CN} atoms. The paramagnetic ligand performs the bridging tridentate function, linking the three centrosymmetric $\{M(hfac)_2\}$ fragments. As a result, in the solid state these compounds have polymer

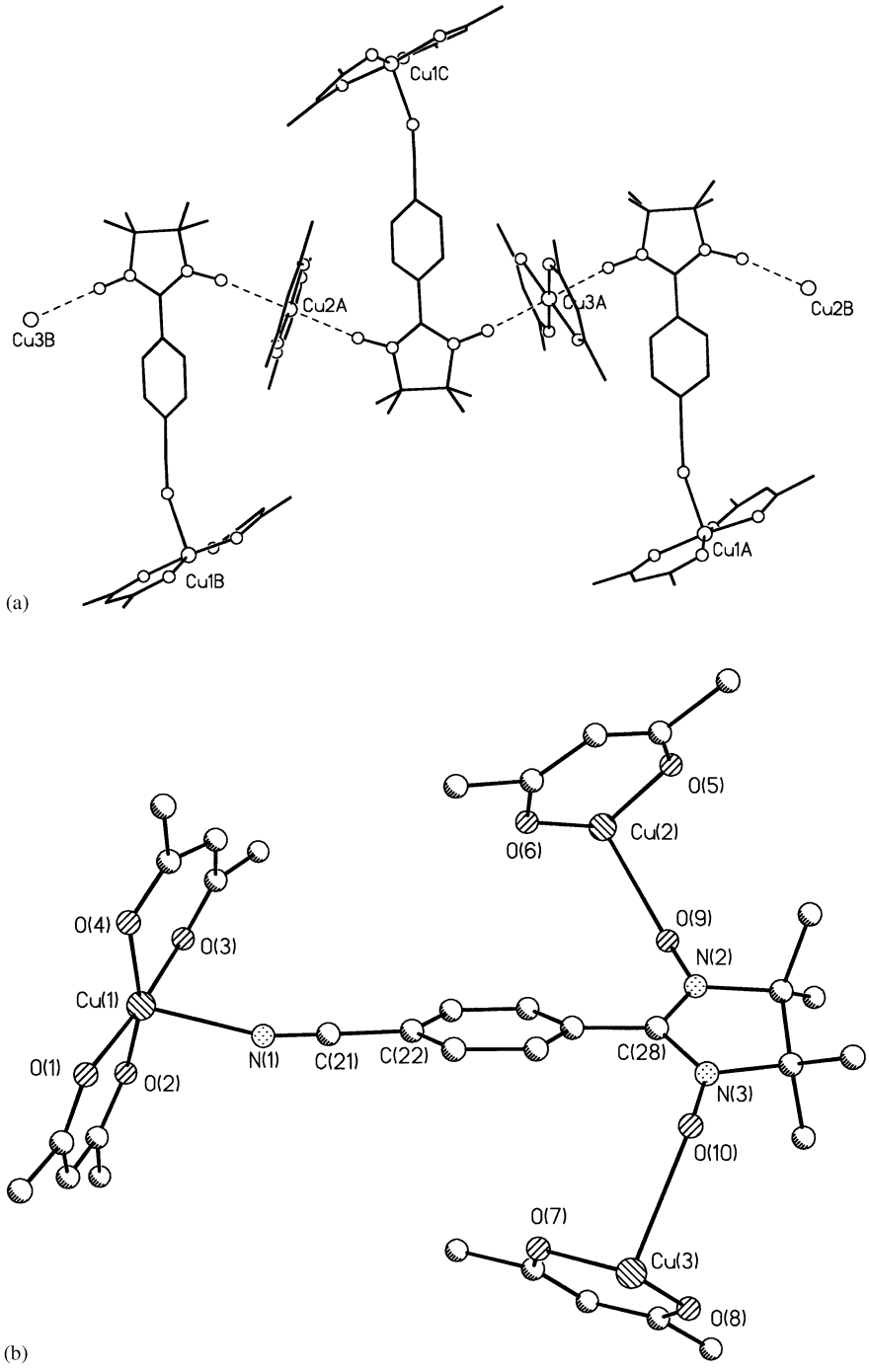

Fig. 2. Chain and atom numbering scheme in the structure of $[Cu(hfac)_2]_2L$.

layers parallel to the (1 1 1) plane. Between the layers, the shortest contacts are F···F (2.871 Å), whose lengths are close to the sum of the van der Waals radii of F atoms.

3.2. Magnetic properties

Magnetic measurements at room temperature gave $\mu_{eff} = 2.48$ B.M., for α- and β-$Cu(hfac)_2L$ (Fig. 4). This is close to the theoretical value of 2.45 B.M. for two weakly coupled spin moments $S = 1/2$. For $[Cu(hfac)_2]_2L$, the analogous value equals 3.12 B.M. (Fig. 4, insert), which is also in good agreement with the theoretical value of 3 B.M. for three weakly coupled magnetic moments $S = 1/2$. At lowered temperatures, μ_{eff} grows for all of the copper compounds, indicating that ferromagnetic exchange interactions along the direct exchange channels $Cu–O^{\bullet}–N<$ inside the chain are predominant. As opposed to α- and β-$Cu(hfac)_2L$, $[Cu(hfac)_2]_2L$ has an extra (indirect) exchange channel

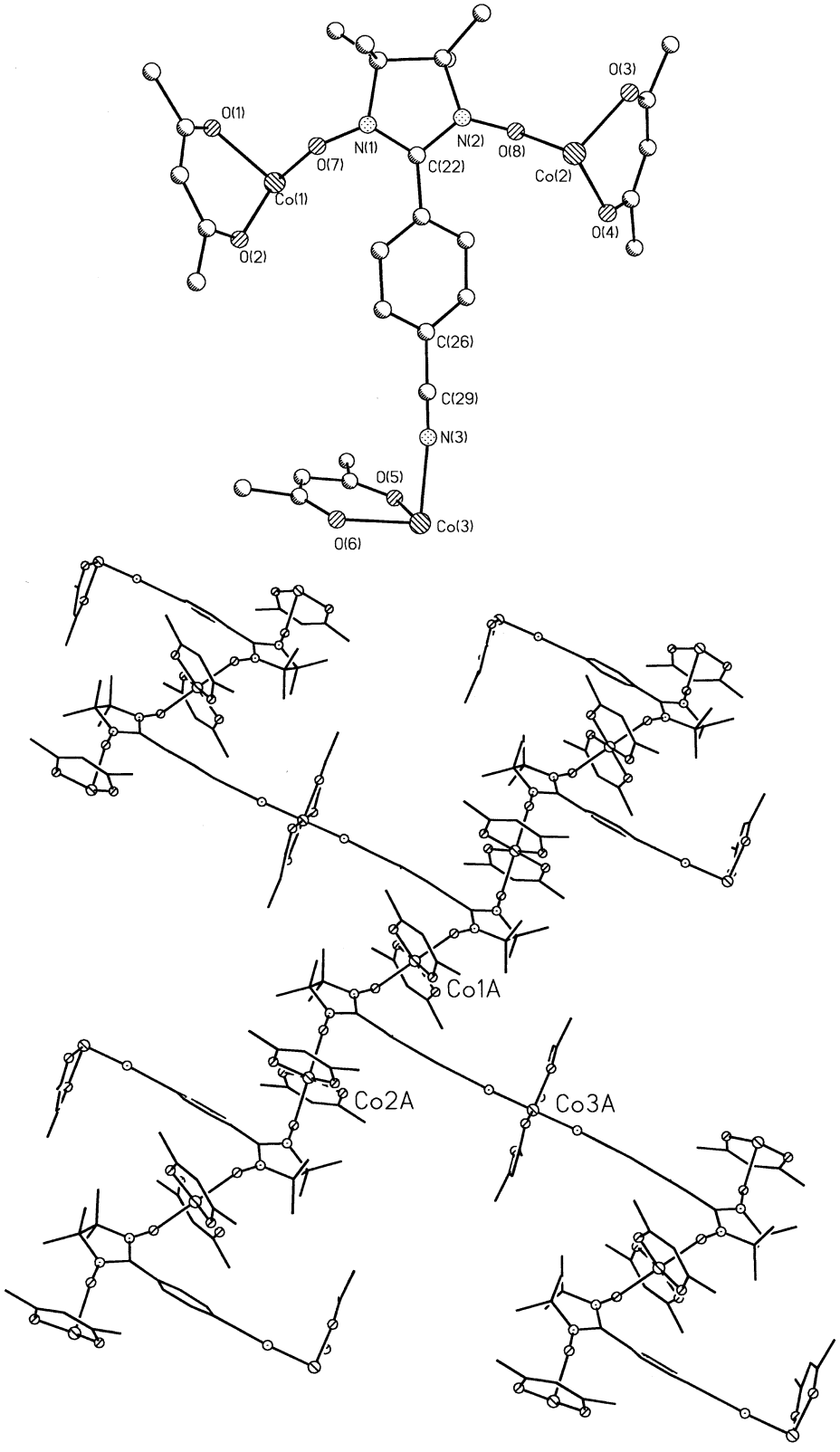

Fig. 3. Numbering scheme and layer formation in $[Co(hfac)_2]_3L_2$.

Cu(II)–N···N–•O of interaction of Cu(II) and nitroxide via the {NC–PhCN} fragment of the ligand, which is much less effective than the direct intrachain channel [4].

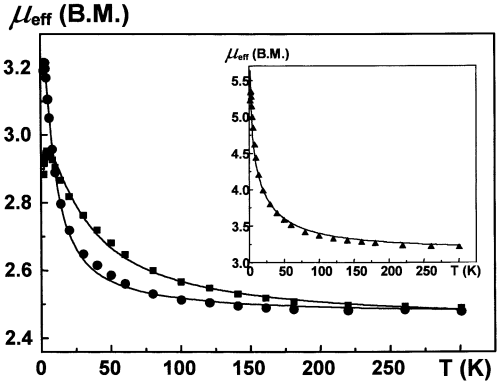

Fig. 4. Temperature dependences of μ_{eff} for α-Cu(hfac)$_2$L (●) β-Cu(hfac)$_2$L (■) and [Cu(hfac)$_2$]$_2$L (insert ▲). Solids—theoretical curves.

The exchange interactions inside the chains in the case of axial coordination by the Cu(II) ion is ferromagnetic, its value depending on the Cu–O$_{NO}$ distance and on the dihedral angle between the equatorial plane of the coordination polyhedron and the plane of the 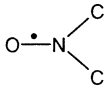 fragment [5–7].

When analyzing the magnetic properties of α-Cu(hfac)$_2$L with an asymmetric axial coordination of the metal (2.697 and 2.488 Å) it is logical to introduce two exchange parameters, J_1 and J_2 (Scheme 2(a)). To evaluate these parameters we used two models describing the experimental dependence $\mu_{eff}(T)$ of the complex. The first is the cluster model, which involves pairs of Cu(II)–O$^{\bullet}$–N< with short axial distances (rectangles in Scheme 2(a)). The value of the J_2 parameter was neglected, assuming it to be small. Using the molecular field technique, the isotropic spin-Hamiltonian including intercluster interactions for this system may be recorded as

$$\hat{H} = -2J_1\hat{s}_{Cu}\hat{s}_R - (g_{Cu}\hat{s}_{Cu} + g_R\hat{s}_R)\beta H - 2nJ'\hat{S}\langle\hat{S}\rangle \qquad (1)$$

where s_{Cu} and s_R are the spins of Cu(II) and nitroxide, g_{Cu} and g_R are the respective g-factors; $S = s_{Cu} + s_R$ is the total spin; nJ' is the intercluster exchange parameter. The theoretical calculation in the framework of this Hamiltonian [5] (g_R was taken to be 2) gave the following optimal parameters: $g_{Cu} = 2.03$, $J_1 = 6.7$ cm^{-1}, and $nJ' = -0.72$ cm^{-1} (for $\sigma = 0.0332$). The second model is an alternate chain suggesting alternation of exchange interactions $J_1 \neq J_2$ 8; this model afforded the following values of parameters: $g_{Cu} = 2.03$, $J_1 = 5.7$ cm^{-1}, $J_2 = 0.35$ cm^{-1}, $nJ' = 0.1$ cm^{-1}, $\sigma = 0.00009$. Since J_1 is much greater than J_2, the cluster model seems to be preferable. In Fig. 4, the curve $\mu_{eff}(T)$ calculated in the framework of the cluster approximation is shown as solid line.

Table 5
Exchange parameters

Model	J_1, cm^{-1}	J_2, cm^{-1}	nJ', cm^{-1}	σ
3a	41.0	–	0.4	0.439
3b	28.2	24.0	0.2	0.099
3c	27.9	19.9	0.07	0.030

In contrast to α-Cu(hfac)$_2$L, the polymer chains of β-Cu(hfac)$_2$L have two short Cu–O$_{NO}$ distances (2.414 Å) sequentially alternating with two longer distances (2.638 Å). The experimental data of this complex are described using the model of a three-center exchange cluster >N–$^{\bullet}$O–Cu(II)–O$^{\bullet}$–N–< with short copper–nitroxide distances (rectangles in Scheme 2(b)). The J_2 interactions were assumed to be essentially weaker. The spin-Hamiltonian of this cluster may be recorded as

$$\hat{H} = -2J\hat{s}_{Cu}\hat{s}' - (g_{Cu}\hat{s}_{Cu} + g_R\hat{s}')\beta H - 2nJ'\hat{S}\langle\hat{S}\rangle \qquad (2)$$

where $s' = s_{R1} + s_{R2}$ is the total spin of the two radicals, and $S = s_{Cu} + s'$ is the spin of the cluster. Taking into account the Cu(II) ions not included in the exchange clusters, the magnetic susceptibility of β-Cu(hfac)$_2$L may be represented as the sum:

$$\chi = \chi_{cl} + \frac{N\beta^2 g_{Cu}^2}{4kT}$$

here the first term, is the magnetic susceptibility of the cluster corresponding to Hamiltonian (Eq. (2)), and the second term is the contribution of the quasiisolated

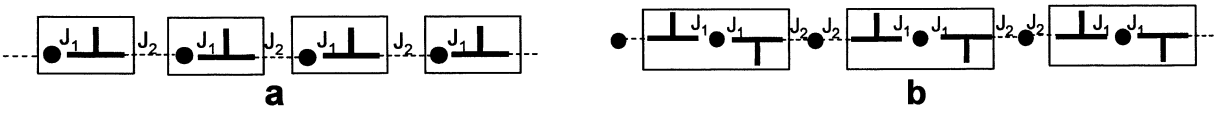

Scheme 2.

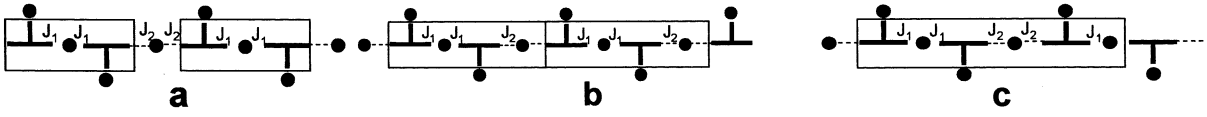

Scheme 3.

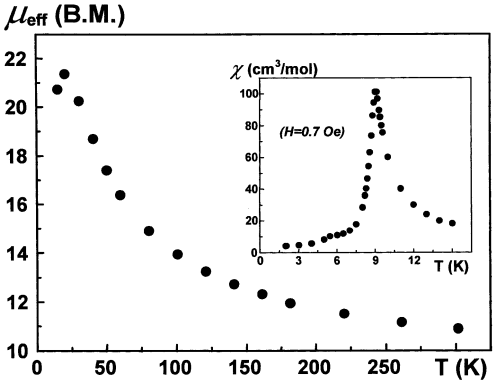

Fig. 5. Dependence $\mu_{eff}(T)$ for the polymeric complex $[Mn(hfac)_2]_3L_2$. Insert—curve $\chi(T)$.

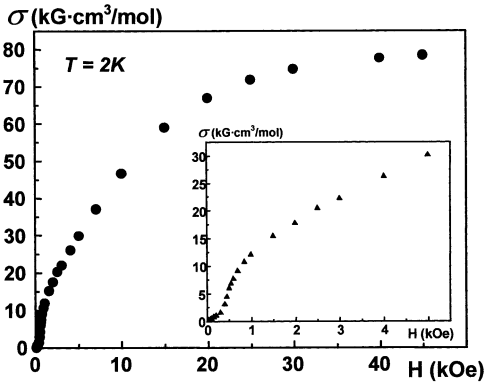

Fig. 7. Magnetization of $[Mn(hfac)_2]_3L_2$.

Cu(II) ions (lying beyond the rectangles in Scheme 2(b)) to magnetic susceptibility. Optimization employing this model yielded the following values of parameters: $g_{Cu} = 2.04$, $J_1 = 8.8\ cm^{-1}$ and $nJ' = -0.03\ cm^{-1}$ ($\sigma = 0.0028$). The theoretical curve corresponding to these parameters is presented in Fig. 4.

To describe the magnetic properties of $[Cu(hfac)_2]_2L$ we used the model of a three-center exchange cluster >N–•O–Cu(II)–O•–N–< and three weakly interacting copper atoms (Scheme 3(a)). Magnetic susceptibility of the complex in this case is the sum:

$$\chi = \chi_{cl} + 3\frac{N\beta^2 g_{Cu}^2}{4kT}$$

Table 5 presents the results of calculations for the model of the clusters depicted in Scheme 3. The varied parameters in this case were J_1 and nJ'. The effective g-factor of Cu(II), equal to 2.13, was determined from the asymptotic value of μ_{eff} at high temperatures. Note that the nJ' parameter is correlated between the intercluster exchange interactions and those interactions (not included in consideration) which involve weakly interacting copper ions and nitroxides. This model inadequately describes experimental data in the low temperature range. This is probably caused by the incorrectness of the condition whereby the J_2 parameter is assumed to be small compared to J_1. Inclusion of the channel of the extra Cu(II) ion with the exchange parameter J_2 in the model cluster (Scheme 3(b and c)) leads to better agreement between the theoretical and experimental data compared to model 2a (Table 5). This result points to a considerable contribution of exchange by the J_2 channel in this complex.

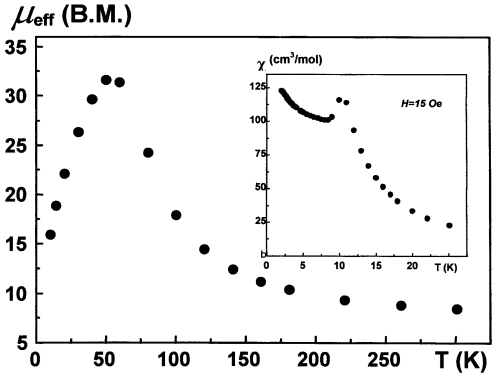

Fig. 6. Dependence $\mu_{eff}(T)$ for the polymeric complex $[Co(hfac)_2]_3L_2$. Insert—curve $\chi(T)$.

In contrast to the above copper complexes, $[M(hfac)_2]_3L_2$ has uniform polymer chains forming layers with equal distances M(II)–O•–N< (Scheme 1(d)). In the case of direct coordination of the metal and nitroxyl groups in such chains, the exchange interactions are antiferromagnetic because of a substantial overlap between the orbitals of the odd electrons of the metal and nitroxyl groups. The energies of these exchange interactions may be $> |300|\ cm^{-1}$ [10]. The off-chain metal atoms linking the chains into layers are involved in indirect interactions with the odd electrons of the nitroxyl groups via the {–PhCN} fragment. The character of this interaction is similar to that of copper complexes considered above. This interaction is ferromagnetic; its energy is up to ~ 1–$2\ cm^{-1}$ [8].

Figs. 5 and 6 present the dependences $\mu_{eff}(T)$ above 15 K for $[M(hfac)_2]_3L_2$ (M = Mn, Co). At lower temperatures, μ_{eff} increases as a consequence of spin correlation with short-range ferrimagnetic ordering in the chains of $[M(hfac)_2]_3L_2$:

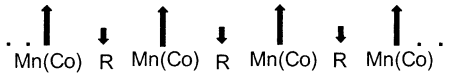

The maxima observed on the $\mu_{eff}(T)$ curves of $[Mn(hfac)_2]_3L_2$ and $[Co(hfac)_2]_3L_2$ at 20 and 50 K are a consequence of the effect of saturation, when magnetic susceptibility at lowered temperature starts to depend on the magnetic field strength. Accordingly, the position of maxima on the temperature axis also depends on the strength of the external magnetic field. As the temperature is lowered further, $[Mn(hfac)_2]_3L_2$ and $[Co(hfac)_2]_3L_2$ pass to the magnetically ordered state at 9.1

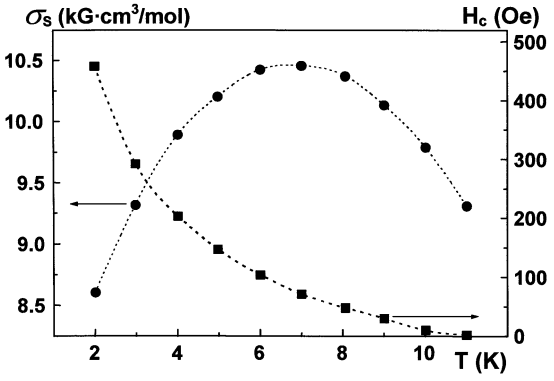

Fig. 8. Temperature dependences of σ_S and H_c for $[Mn(hfac)_2]_3L_2$.

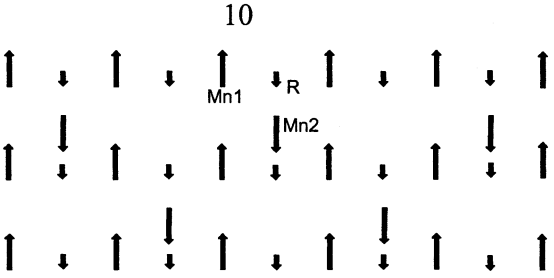

Scheme 4.

and 11.9 K, respectively, as indicated by the anomalies on the curves $\chi(T)$ measured in low magnetic fields (Figs. 5 and 6, inserts).

In the region below the phase transition temperature, the field dependences of magnetization $\sigma(H)$ for $[Mn(hfac)_2]_3L_2$ have a complex form. Fig. 7 shows an isotherm $\sigma(H)$ at 2 K. No hysteresis was recorded within the experimental error when magnetization reversal took place. The behavior of magnetization in magnetic fields of up to 0.05 T (Fig. 7, insert) is characterized by an abrupt change in a critical magnetic field H_c equal to 0.046 T. Above it is a small linear section defined by the relation $\sigma(H) = \sigma_S + \chi H$, where spontaneous magnetization σ_S equals $\sim 10^4$ G cm^3 mol^{-1} at 2 K. In higher fields (up to 4.5 K), magnetization increases, tending to the value of 78 400 G cm^3 mol^{-1}, which is close to the saturation limit $Ng\beta S = 72\,605$ G cm^3 mol^{-1} for the total spin $S = 13/2$

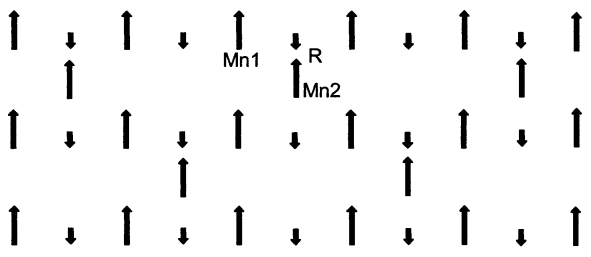

Scheme 5.

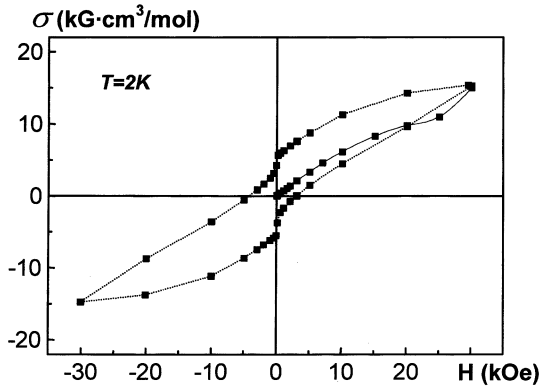

Fig. 9. Magnetization and hysteresis of $[Co(hfac)_2]_3L_2$.

($g = 2$) per complex molecule. The experimental dependences σ_S and $H_c(T)$ are given in Fig. 8.

Based on the data obtained, the qualitative picture of ferrimagnetic ordering in a polymer layer may be represented as shown in Scheme 4, reflecting the anti ferromagnetic interactions of Mn1 ions and nitroxides R in chains, as well as ferromagnetic interactions of Mn2 ions and two R between chains. Magnetization of a layer of this kind for $[Mn(hfac)_2]_3L_2$ is $\sigma = 2\sigma(Mn1) - \sigma(Mn2) - 2\sigma(R)$, which equals $\sim 16.8 \times 10^3$ G cm^3 mol^{-1}, corresponding to $S = 3/2$ per complex molecule.

In magnetic fields lower than H_c in $[Mn(hfac)_2]_3L_2$, antiferromagnetic interactions between layers form an antiferromagnetic structure, in which the magnetic moments of the ferrimagnetically ordered (Scheme 4) neighboring layers are antiparallel. When $H = H_c$, a metamagnetic transition occurs. The magnetic moments of half of all layers oriented oppositely to the field are reversed. The jump in magnetization must be $\sim 16.8 \times 10^3$ G cm^3 mol^{-1} (at 0 K). The experimental value of the jump is slightly smaller, $\sim 10^4$ G cm^3 mol^{-1} at 2 K. One of the reasons for this discrepancy is polycrystallinity of the sample. In a magnetic field above 1.5–2.0 T, the magnetic moments of weakly interacting Mn2 ions (Scheme 4) inside the polymer layers turn in the direction of net magnetization, forming the following magnetic structure:Scheme 5

The value of magnetization of $[Mn(hfac)_2]_3L_2$ will tend to the sum $2\sigma(Mn1) + \sigma(Mn2) - 2\sigma(R)$, which equals 72 605 G cm^3 mol^{-1} and corresponds to the spin $S = 13/2$ per complex molecule. The experimental value of saturation magnetization is 78 400 G cm^3 mol^{-1}, which is in good agreement with the calculated value. This is evidence in favor of the proposed scheme of magnetic ordering in $[Mn(hfac)_2]_3L_2$.

The field dependences of magnetization for $[Co(hfac)_2]_3L_2$ are more complex than those of $[Mn(hfac)_2]_3L_2$ (Fig. 9). In higher magnetic fields, the curve $\sigma(H)$ shows an inflection, and subsequent magnetization reversal leads to a hysteresis. Note that sample cooling in a weak magnetic field and further magnetization measurements

in magnetic fields of up to 1.5 T lead to a linear dependence $\sigma(H)$ without hysteresis effects. One can assert that the ground state in the magnetically ordered phase of $[Co(hfac)_2]_3L_2$ is also antiferromagnetic and that the scheme of magnetic ordering presented above for $[Mn(hfac)_2]_3L_2$ is also valid for $[Co(hfac)_2]_3L_2$. The critical field of the metamagnetic transition in $[Co(hfac)_2]_3L_2$ is shifted to the region of higher magnetic fields, ~ 3 T (Fig. 9). The jump in magnetization in this case was $\sim 5 \times 10^3$ G cm^3 mol^{-1}; this is in full agreement with Scheme 4 if Mn(II) ions are replaced by Co(II) ions with $S = 3/2$. The presence of a hysteresis as well as the dependence of measurement data on the mode of heating and cooling in a magnetic field are primarily associated with high magnetic anisotropy characteristic of the octahedral Co(II) ion. The presence of a hysteresis and its parameters may be of microscopic nature, or they may be due to macroscopic factors associated with polycrystallinity of the sample.

Thus layered polymers $[Mn(hfac)_2]_3L_2$ and $[Co(hfac)_2]_3L_2$ are new examples of molecular magnets exhibiting cooperative magnetic ordering effects at 9.1 and 11.9 K, respectively.

4. Supplementary material

Crystal data for structural analysis of α-, β-$Cu(hfac)_2L$, $[Cu(hfac)_2]_2L$, $[Mn(hfac)_2]_3L_2$ and $[Co(hfac)_2]_3L_2$ have been deposited with the Cambridge Crystallographic Data Centre, CCDC Nos. 203052–203057. Copies of this information may be obtained free of charge from The Director, CCDC, 12 Union Road, Cambridge, CB2 1EZ, UK (fax: +44-1223-336033; e-mail: deposit@ccdc.cam.ac.uk or www: http://www.ccdc.cam.ac.uk).

Acknowledgements

Research funded in part by US Civilian and Development Foundation (grant REC-008), RFBR (grants 00-03-32987, 02-03-33112), Minobr RF (grants E00-50-80, E02-5.0-188) and Siberian Branch of RAS.

References

[1] O.V. Koreneva, G.V. Romanenko, V.N. Ikorskii, S.V. Fokin, V.I. Ovcharenko, J. Struct. Chem. 42 (2001) 977.
[2] V. Ovcharenko, S. Fokin, P. Rey, Mol. Cryst. Liq. Cryst. 334 (1999) 109.
[3] V.I. Ovcharenko, S.V. Fokin, G.V. Romanenko, I.V. Korobkov, P. Rey, Russ. Chem. Bull. 48 (1999) 1519.
[4] F. Lamfranc de Panthou, D. Luneau, R. Musin, L. Ohrstrom, A. Grant, P. Turek, P. Rey, Inorg. Chem. 35 (1996) 3484.
[5] I.V. Ovcharenko, Yu.G. Shvedenkov, R.N. Musin, V.N. Ikorskii, J. Struct. Chem. 40 (1999) 29.
[6] R.N. Musin, P.V. Schastnev, S.A. Malinovskaya, Inorg. Chem. 31 (1992) 4118.
[7] V.I. Ovcharenko, A.B. Burdukov, R.N. Musin, Mol. Cryst. Liq. Cryst. 273 (1995) 89.
[8] A.B. Gelman, V.N. Ikorskii, Zh. Strukt. Khim. 30 (4) (1977) 81.
[9] A. Caneschi, D. Gatteschi, A. Lirzin, Mat. Chem. 4 (2) (1994) 319.
[10] A. Caneschi, D. Gatteschi, R. Sessoli, P. Rey, Inorg. Chim. Acta 184 (1991) 67.